analytical chemistry

pubs.acs.org/ac Article

Designed Three-in-One Peptides with Anchoring, Antifouling, and Recognizing Capabilities for Highly Sensitive and Low-Fouling Electrochemical Sensing in Complex Biological Media

Zhen Song, Min Chen, Caifeng Ding, and Xiliang Luo*

Cite This: *Anal. Chem.* 2020, 92, 5795−5802 Read Online

ACCESS | Metrics & More | Article Recommendations | Supporting Information

ABSTRACT: Nonspecific adsorption is of great concern for electrochemical biosensors performing in complex biological media, and various antifouling materials have been introduced into the sensing interfaces to improve the antifouling capability of different biosensors. However, for most of the biosensors with antifouling materials and sensing probes coexisting in the sensing interfaces, either the antifouling materials will impair the sensing performances or the sensing probes will affect the antifouling ability. Herein, a facile and efficient antifouling biosensor was developed based on a newly designed three-in-one peptide with anchoring, antifouling, and recognizing capabilities. One end of the designed peptide is a unique anchoring part that is rich in amine groups, and this part can be anchored to the poly(3,4-ethylenedioxythiophene) (PEDOT)-citrate film electrodeposited on a glassy carbon electrode. The other end of the peptide is a recognizing part that can specifically bind to the aminopeptidase N (APN) and human hepatocellular carcinoma cells (HepG2 cells). Meanwhile, the middle part of the peptide, together with the anchoring part, was designed to be antifouling. With this designed multifunctional peptide, highly sensitive and low-fouling biosensors capable of assaying target APN and HepG2 cells in complex biological media can be easily prepared, with detection limits of 0.4 ng·mL^{-1} and 20 cells·mL^{-1}, respectively. This antifouling biosensor is feasible for practical target detection in real complex samples, and it is highly expected that this peptide designing strategy may be extended to the development of various antifouling biosensors.

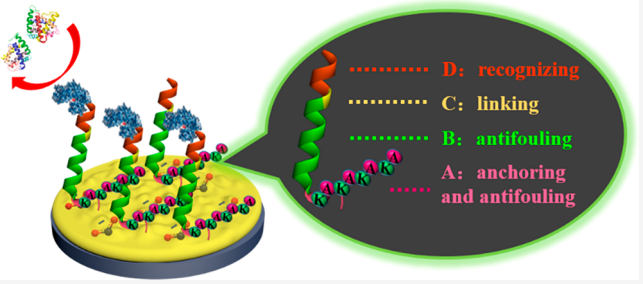

Local and systemic fouling is a serious problem in the field of biosensors, and it limits the practical application of biosensors in natural and complex biological media, such as human blood and serum.[1−3] Such fouling, which arises from nonspecific protein adsorption, severely influences the reliability and stability of sensors for direct detection in biological samples.[4,5] Therefore, the development of antifouling biosensors that can effectively reduce nonspecific adsorption to maintain biosensor performances has fueled extreme interest. To construct antifouling biosensors, the sensing interfaces are normally modified with certain kinds of antifouling materials, especially poly(ethylene glycol) (PEG)[1,6] and oligo(ethylene glycol) (OEG),[7] which were considered "gold standard" materials.[8] PEG and OEG are effective coating materials that can prevent nonspecific protein adsorption,[1,6,9] but they also have some flaws including oxidative damage, poor water solubility, and low protein resistance at high temperature.[10−13]

Peptides have emerged as potential alternative antifouling materials with the additional advantages of biocompatibility, tunable structure, and facile synthesis.[3,14−16] A variety of antifouling peptide sequences have been reported. For example, Jiang's group has designed an antifouling peptide (EKEKEKE-PPPPC)[14] that consists of alternating positively charged lysine (K) and negatively charged glutamic acid (E), proving that the peptide exhibited excellent performance to resist the protein adsorption. A new sequence (EESK-SESKSGGGGC)[3] designed by Cui and co-workers showed a similar antifouling property. Our group has also investigated the antifouling branched peptides (CPPPPEK2(EK)4(EK)),[8] which showed properties that are superior to those of linear structural peptides. Although these peptide sequences proved to have good antifouling performances, they were mainly immobilized on surfaces through complicated chemical reactions or self-assembly on limited metal surfaces like Au, and sometimes additional blocking regents were used to block the peptide-modified interface.[17] Recently, a self-assembled layer of oligopeptides (AKAKAKAK),[18] which carries positive charges, was reported to be able to cover the negatively

Received: November 22, 2019
Accepted: March 19, 2020
Published: March 19, 2020

https://dx.doi.org/10.1021/acs.analchem.9b05299
Anal. Chem. 2020, 92, 5795−5802

Scheme 1. Fabrication Process of the Antifouling Biosensor Based on Designed Three-in-One Peptide

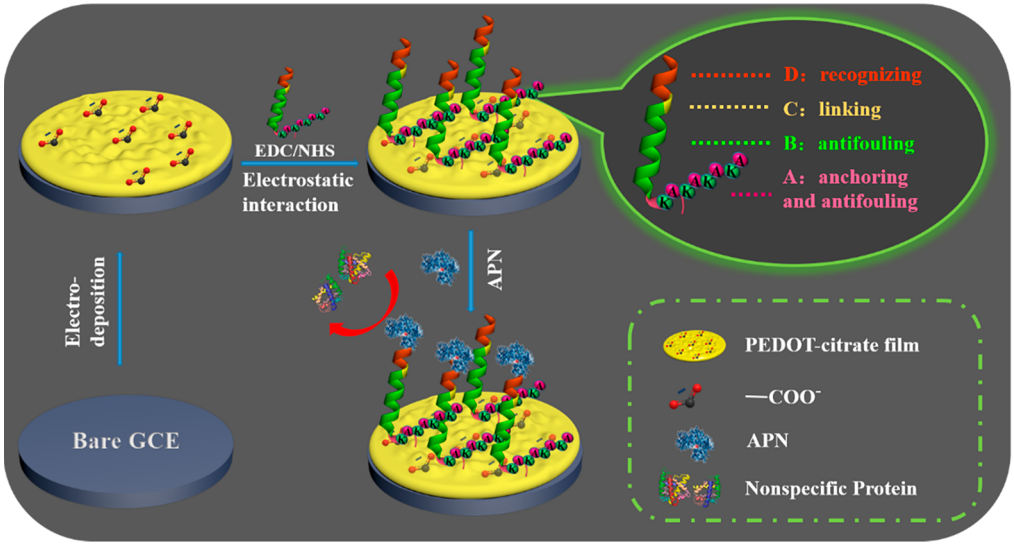

charged surface well by self-organizing into a compact amphipathic layer to prevent the biofouling. These self-assembled oligopeptides may be combined with other common linear antifouling peptides through reasonable structural design to achieve better antifouling performances.

Some peptides were also found to be good small-molecule ligands or receptors. It was reported that RGD (arginine-glycine-aspartate)[14,19,20] could selectively bind to tumor cells, and a peptide sequence (HWRGWVA)[15,21,22] was used to detect the IgG. Wang and co-workers have proposed a novel sequence (YVEYHLC)[23] that possessed nanomolar affinity and specific recognition for aminopeptidase N (APN) both in vivo and in vitro. APN is known as a membrane protein[24] and participates in many physiological processes, such as immunological response, signal transduction, and antigen reaction,[25] broadly in human organs and tissues. APN plays an important role in proliferation, invasion, and angiogenesis of tumors,[26−29] and it can be identified as a cancer biomarker for early diagnosing and judging the prognosis of cancer.[30,31] To date, fluorescence spectroscopy[32,33] is the most common method for the detection of APN, but it has high background signal and needs expensive instruments.

Because of its simple operation, rapid response, and high sensitivity,[34] electrochemistry has become an ideal detection method. Herein, we fabricated an antifouling electrochemical biosensor based on a newly designed peptide (YVEYHLCREKEKEKEKAKAKAKAK) anchored to a conducting polymer-modified electrode, as displayed in Scheme 1. The designed peptide has four domains: anchoring and antifouling (AKAKAKAK), antifouling (EKEKEKEK), linking (R, which balanced the negative charge of the recognizing part), and recognizing (YVEYHLC). The positively charged sequence AKAKAKAK can adsorb on the negatively charged poly(3,4-ethylenedioxythiophene) (PEDOT)-citrate film. The recognizing sequence can ensure specific binding to APN and human hepatocellular carcinoma cells (HepG2 cells; APN overexpressed in cytomembrane).[32,33] The antifouling sequence and the anchoring sequence are linked through rational design, and these two sequences are overall antifouling as a whole. On the basis of this designed three-in-one peptide combined with anchoring, antifouling, and recognizing capabilities, highly sensitive and low-fouling electrochemical biosensors were successfully discovered and applied in the assaying of APN and HepG2 cells in complex media.

EXPERIMENTAL SECTION

Materials and Reagents. Newly designed peptides ($peptide_3$, YVEYHLCREKEKEKEKAKAKAKAK) as well as $peptide_1$ and $peptide_2$ (YVEYHLCRAKAKAKAK and YVEYHLCREKEKEKEK, respectively) were designed by our group and synthesized by Bankpeptide Biological Technology Co., Ltd. (Hefei, China). APN was purchased from R&D Systems. Sodium citrate, glutathione (GSH), 3,4-ethylenedioxythiophene (EDOT), and hexaammineruthenium(III) chloride ($Cl_3H_{18}N_6Ru$) were ordered from Aladdin Reagents (Shanghai, China). *N*-Hydroxysuccinimide (NHS), 1-ethyl-3-(3-dimethylaminopropyl) carbodiimide (EDC), and fluorescein diacetate (FDA) were ordered from Sigma-Aldrich. Fetal bovine serum (FBS), human serum albumin (HSA), myoglobin (Mb), lysozyme (LYS), and albumin (BSA) were obtained from Beijing Bo Yang Hongda Technology Co., Ltd. (Beijing, China). Human serum samples from volunteers were collected by the Eighth People's Hospital of Qingdao (Qingdao, China), and the informed consent for use of the human serum was obtained. All the sample preparation was authorized by the institutional review board of the Eighth People's Hospital of Qingdao and was performed in compliance with the institutional guidelines and relevant laws. Other chemical reagents were of analytical grade. Deionized water (DI water, 18 MΩ/cm) was provided with a Milli-Q water-purification system and used for preparing all aqueous solution. Phosphate-buffered saline solution (PBS, pH 7.4, 10 mM) was used for the preparation of peptide solution and washing buffer solution.

Apparatus and Measurements. Scanning electron microscopy (SEM) characterizations were carried out with a Hitachi S-4800 scanning electron microscope (Hitachi Co., Japan). The confocal images were performed with the TCS SP5 confocal laser microscope (Leica, Germany). An ESCALAB 250Xi spectrometer (Thermo Fisher Scientific, U.K.) instrument was used for X-ray photoelectron spectroscopy (XPS) analysis with a monochromatic Al Kα X-ray source, and all spectra were calibrated by normalizing the

https://dx.doi.org/10.1021/acs.analchem.9b05299
Anal. Chem. 2020, 92, 5795−5802

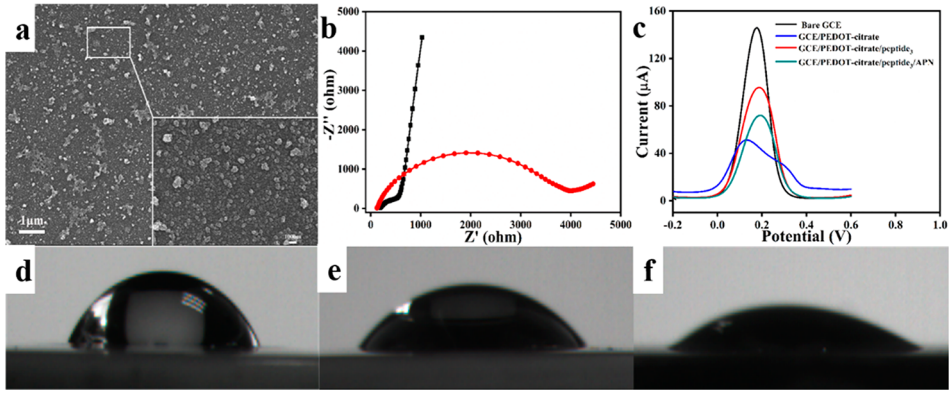

Figure 1. (a) SEM images of the PEDOT-citrate film; inset shows partial enlargement. (b) Nyquist plots of the EIS for the GCE/PEDOT-citrate in the presence of 5.0 mM $Fe(CN)_6^{3-/4-}$ (red curve) and $[Ru(NH_3)_6]^{3+}$ (black curve) with 0.1 M KCl as electrolyte. (c) DPV curves recorded at different modified electrodes in PBS (10 mM, pH 7.4) containing 5.0 mM $[Fe(CN)_6]^{3-/4-}$ and 0.1 M KCl. Contact angle images of bare GCE (d), GCE/PEDOT-citrate (e), and GCE/PEDOT-citrate/$peptide_3$ (f).

C(1s) peak to the standard value of 284.6 eV. Zeta potential of the peptide was tested by a Zetasizer Nano-ZS (Malvern Instruments, Malvern, U.K.). Surface wettabilities of the modified electrodes were measured by a contact angle measuring instrument (JC2000 Shanghai Zhongchen instrument Co., China). Fourier transform infrared (FT-IR) spectra were collected with the ATR-FT-IR Nicolet iS10 spectrometer made by Thermo Fisher (American).

Electrochemical experiments were performed with a CHI 760D electrochemical workstation (Shanghai Chenhua Instrument Co., Ltd., China) at room temperature. A conventional three-electrode system with a platinum wire as the counter electrode, a saturated calomel electrode (SCE) as the reference electrode, and a bare or modified glassy carbon electrode (GCE, 3.0 mm in diameter) as the working electrode was used. Differential pulse voltammetry (DPV), cyclic voltammetry (CV), and electrochemical impedance spectroscopy (EIS) detection were carried out in phosphate-buffered saline solution (PBS, 10 mM, pH 7.4) containing 5.0 mM $[Fe(CN)_6]^{3-/4-}$ or 5.0 mM $[Ru(NH_6)_3]^{3+}$ and 0.1 M KCl. CV was recorded with a potential range from −0.2 to 0.6 V and a scan rate of 100 mV·s^{-1}. DPV was recorded with an amplitude of 50 mV and a potential range from −0.2 to 0.6 V. EIS was recorded at a frequency range of 0.1 Hz to 100 kHz with the current potential set as 0.2 V.

Synthesis of PEDOT-Citrate/Peptide Interface. Prior to synthesis of the PEDOT-citrate films, the bare glassy carbon electrodes (GCEs) were polished with alumina slurries with particle sizes of 0.3 and 0.05 μm successively and then cleaned by water, absolute ethanol, and water for 2 min under ultrasonic conditions in sequence. The PEDOT-citrate films were fabricated according to a previous method.[35] First, 0.02 M PEDOT and 0.0434 g of sodium citrate, which acts as a negative dopant during the electrodeposition of PEDOT, were added into 5.0 mL of deionized water by an ultrasonic dispersion. The electrodeposition of PEDOT and citrate was performed on a bare GCE at a potential of 1.1 V (vs SCE) for 200 s.

The peptides were immobilized on PEDOT-citrate films by two kinds of forces. On one hand, carboxyl groups on the PEDOT-citrate films and amino groups on the peptides can form covalent bonds with the assistance of EDC/NHS. On the other hand, the short positively charged part of peptides (AKAKAKAK) can anchor to the negatively charged PEDOT-citrate films through electrostatic attraction. Specific immobilization steps are as follows: First, the PEDOT-citrate film-modified electrodes were soaked in a solution (pH 5.5) containing 0.2 M EDC and 0.1 M NHS for 30 min and then gently washed with deionized water. Second, 10 μL of 50 μM peptide solution was dropped on the surface of the modified electrodes for 2 h at room temperature, and during this process the electrode was covered with a wet beaker to keep the electrode surface moist. Third, after washing with phosphate-buffered saline (PBS, 10 mM, pH 7.4), the biosensor interface (GCE/PEDOT-citrate/peptide) was obtained, and it was stored at 4 °C before use.

Surface Property Evaluation. To evaluate the property of the PEDOT-citrate film-modified electrodes, the water contact angle was tested in different solutions (pH: 1, 4, 7, 11) by a static water contact angle (WCA) measurement. In addition, EIS and DPV measurements were employed using negatively charged $[Fe(CN)_6]^{3-/4-}$ and positively charged $[Ru(NH_3)_6]^{3+}$ probes.

Characterization of the Designed Peptide. Attenuated total reflectance FT-IR (ATR-FT-IR) spectroscopy was used to analyze the secondary structure of designed peptides, scanning from 1300 to 1800 cm^{-1}. The electrical property of the peptides was obtained by theoretical calculation and measured by a Zetasizer Nano-ZS (Malvern Instruments, Malvern, U.K.). Zeta potential was recorded in 1 mg·mL^{-1} peptide aqueous solution.

Antifouling Assessments. The antifouling properties of the modified electrodes were tested in several single-protein solutions and complex biological samples. DPV signals were recorded to monitor the change of the electrode surfaces before and after incubation in protein and biological solutions. Protein solutions and the complex biological samples were diluted by PBS (10 mM, pH 7.4).

Cell Incubation and Fluorescence Imaging. The HepG2 cells (human hepatocellular carcinoma cells) and HeLa cells (human cervical cancer cells), which were ordered from Procell Life Science & Technology Co., Ltd. (Wuhan, China), were cultured in DMEM (Dulbecco's modified Eagle's medium, Sigma-Aldrich) supplemented with 10% FBS (fetal bovine serum), 1% streptomycin, and 1% penicillin at 37 °C incubator under 5% CO_2 atmosphere. Culture solution was changed every 2 days. At the logarithmic growth phase, cells were digested using Dulbecco's phosphate-buffered saline (D-

https://dx.doi.org/10.1021/acs.analchem.9b05299
Anal. Chem. 2020, 92, 5795−5802

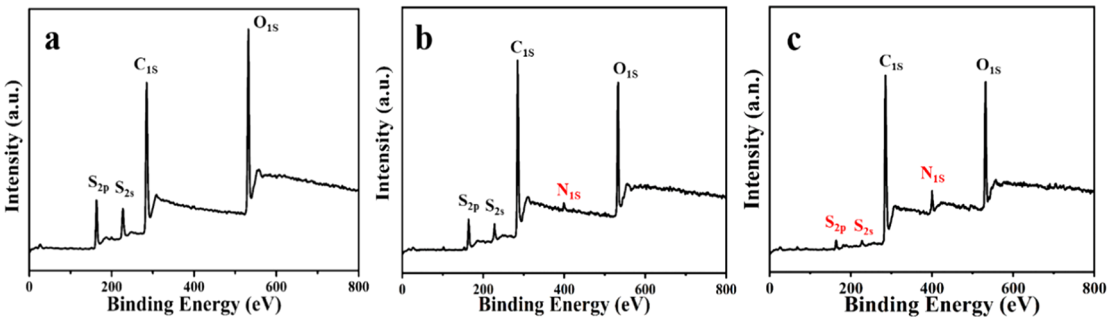

Figure 2. Full-scan XPS spectra of the GCE/PEDOT-citrate (a), GCE/PEDOT-citrate/peptide$_3$ (b), and GCE/PEDOT-citrate/peptide$_3$/APN (c) electrodes.

PBS) containing 0.25% trypsin and 0.02% EDTA and then centrifuged at 1000 rpm for 5 min. The cells were collected and washed with D-PBS, and then a homogeneous suspension in D-PBS was obtained. The cell number was recorded by a Petroff−Hausser cell counter. For fluorescence imaging, the cells were incubated in fluorescein diacetate (FDA) solution (50.0 μg·mL^{-1}) in a dark environment for 5 min and washed with PBS. Then cell imaging was performed by a Bruker Tensor 70 spectrometer with 488 nm excitation.

Sensing of APN and HepG2 Cells. The modified electrodes (GCE/PEDOT-citrate/peptide$_3$) were incubated in APN solutions with various concentrations at 37 °C for 1.5 h and then washed with PBS to remove the noncaptured APN. The cell sensing experiments were conducted in HepG2 cells (APN overexpressed in cytomembrane) solutions. The DPV signals were recorded before and after the target binding.

RESULTS AND DISCUSSION

Characterization of the PEDOT-Citrate Film-Modified Electrodes. The micromorphology of the PEDOT-citrate film was monitored by SEM. After PEDOT-citrate electrodepositing on the bare GCE, a uniform but rough film was scattered on the electrode, as shown in Figure 1a. The charge of the PEDOT-citrate film is very important for peptide immobilization. As seen in Figure 1b, the charge-transfer resistance (R_{ct}) of the PEDOT-citrate film-modified electrode in negatively charged $[Fe(CN)_6]^{3-/4-}$ probes (red curve) is larger than that in the positively charged $[Ru(NH_3)_6]^{3+}$ probes (black curve). It may be that some free carboxyl groups, which come from citrate ions, make the electrode surface negatively charged. Because like charges repel but opposite charges attract, there is a strong electrostatic repulsion between the electrode surface and $[Fe(CN)_6]^{3-/4-}$ while there is an electrostatic attraction between the electrode surface and $[Ru(NH_3)_6]^{3+}$; thus, the charge-transfer resistance (R_{ct}) showed the big difference between these two probes. To further prove the presence of the carboxyl groups, the contact angles were recorded in solutions with various pH values. As shown in Figure S1, the contact angle of the PEDOT-citrate film-modified electrode gradually became smaller with the increase in pH from 1 to 11, reflecting that carboxyl groups have two forms, one of which is −COOH in low pH and the other of which is $-COO^-$ in high pH, making the surface more hydrophilic. All these results indicate that the PEDOT-citrate film is negatively charged owing to the presence of carboxyl groups on its surface.

Characterization of the Peptides. Some peptides that are highly hydrophilic and neutral in charge can prevent the protein adsorption. Here the antifouling and recognizing parts were connected through a positively charged arginine, which was used to balance the negative charge of the recognizing part. The isoelectric point (pI) of the sequence (YVEYHL-CREKEKEKEK) is 7.1. Free ε-NH_2 groups in part A of the designed peptide (Scheme 1) are positively charged, so the whole peptide is also positive. The pI of peptide$_3$ is 10.0, and the relationship between net charge of the peptide and pH was recorded, where (Figure S2A) peptide$_3$ has four groups with net charges at pH 7. As displayed in Figure S2B, the zeta potential of the peptide is +57.3 mV, which is closely consistent with the pI and net charge (pH 7) result. The secondary structure of the peptides was analyzed by ATR-FT-IR spectroscopy. As we all know, the secondary structure of peptides could be inferred by amide I band (at 1600−1700 cm^{-1}).[18] As shown in Figure S3, the PEDOT-citrate film-coated surface showed no obvious peaks in this region. Meanwhile, for the peptide-modified PEDOT-citrate film, new bands were observed at 1685 and 1627 cm^{-1}, which were ascribed to the β-turns and β-sheets. Figure S4 shows the structure of the designed peptide, and it is clear that abundant amine groups are present in the positively charged AKAKAKAK part. These amine groups can react with carboxyl groups in the PEDOT-citrate film with the assistance of EDC/NHS, and the unreacted amine groups in this part of the peptide can be immobilized on the electrode surface through the electrostatic attraction.[18]

Characterization of the Biosensor Assembly Process. The assembly process of the APN biosensor was illustrated in Scheme 1. DPV measurement was used to record every fabrication step, as exhibited in Figure 1c. The bare electrode had a large peak current. After electrodeposition of PEDOT-citrate, the peak current decreased significantly due to the electrostatic repulsive force between the negative PEDOT-citrate film and the negatively charged $[Fe(CN)_6]^{3-/4-}$ probes and the moderate electrical conductivity of the polymer film. After the modification with peptides, the peak currents of the modified electrodes increased, due to the fact that the negative charge of the PEDOT-citrate film can be neutralized by the positively charged peptides; therefore, the electrostatic repulsive force to the negative probes will diminish or even disappear. When the electrodes were incubated with target APN, the current responses decreased accordingly, suggesting that the recognition reaction occurred successfully, and the attached APN blocked the electron transfer of the redox probe. To further characterize this process, a positively charged probe ($[Ru(NH_3)_6]^{3+}$) was chosen as the redox probe to record the DPV current change. As displayed in Figure S5B, PEDOT-citrate, peptide, and APN were successively modified on the

https://dx.doi.org/10.1021/acs.analchem.9b05299
Anal. Chem. 2020, 92, 5795−5802

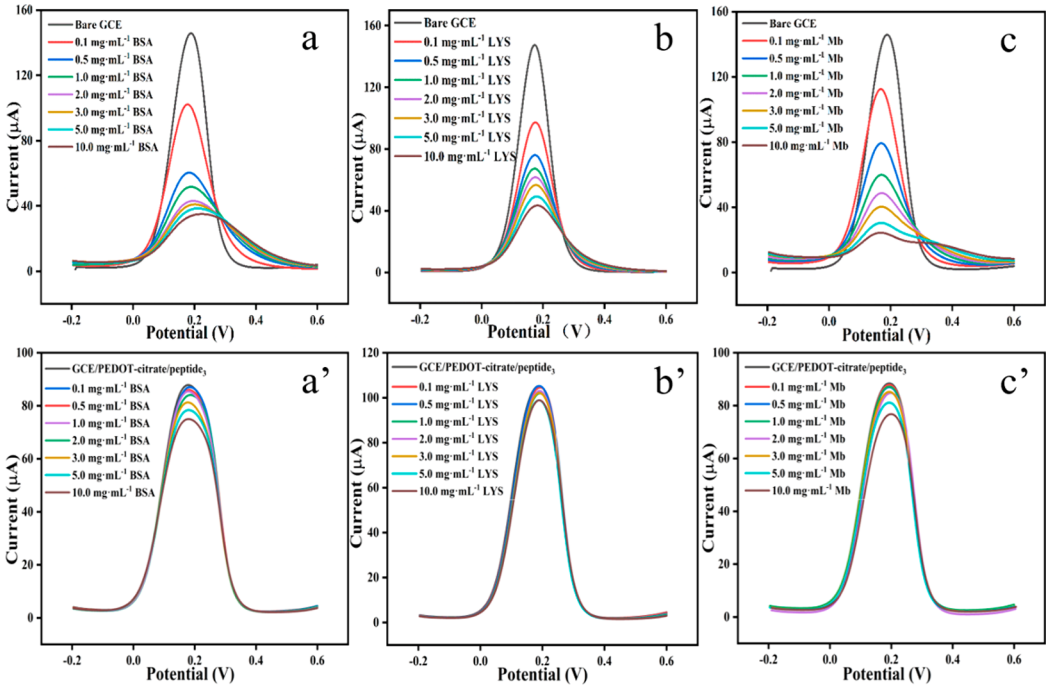

Figure 3. DPV responses of the bare (first line) and PEDOT-citrate/peptide$_3$ (second line) modified GCE after incubation in different concentrations of BSA (a, a′), LYS (b, b′), and Mb (c, c′) solutions. DPV were recorded in PBS (10 mM, pH 7.4) solution containing 5.0 mM $[Fe(CN)_6]^{3-/4-}$ and 0.1 M KCl.

bare GCE, and gradual decreases in DPV peak currents were observed. Because there is no electrostatic repulsion between PEDOT-citrate and positively charged $[Ru(NH_3)_6]^{3+}$ probes, and the peptides and APN are not conductive, the DPV response continuously decreased, which was different from those observed when negatively charged $[Fe(CN)_6]^{3-/4-}$ probes were used.

Meanwhile, changes in surface hydrophilicity were also measured. As shown in Figure 1d–f and Table S1, the bare GCE displayed a contact angle of 63.01°, and after PEDOT-citrate and the three-in-one peptides modifications, the contact angles decreased to 46.73° and 29.24°, respectively. The water contact angle measurement indicated that the PEDOT-citrate/peptide-modified electrode surface possesses good hydrophilicity, which is preferred for antifouling performance.

Besides, the XPS characterizations were performed (Figure 2) to further monitor the biosensor-fabrication process. As displayed in Figure 2a, the PEDOT-citrate-modified GCE was mainly composed of carbon (C), oxygen (O), and sulfur (S) elements. After peptide$_3$ modification, the new typical XPS peak for N 1s appeared, and the S 2p and S 2s decreased (Figure 2b). After incubation in APN, the N 1s peak raised and the S 2p and S 2s peaks further decreased (Figure 2c), indicating that APN molecules were specifically attached to the peptides modified on the electrode surface.

Optimization of Experimental Conditions. To obtain excellent sensing performance, several experimental conditions were investigated. The influence of the peptide concentration and the hybridization time were recorded in detail. As shown in Figure S6a, with the increasing of peptide concentration, the change in the current signal also increases (from 15 to 50 μM) before reaching a stable reading. Hence, the 50 μM peptide was chosen as the optimum concentration in the following experiments. Figure S6b showed that the current signal improved with the reaction time from 30 to 90 min and then tended to level off. Thus, the optimal hybridization time was selected as 90 min.

Antifouling Property. To test the antifouling property of the designed peptide, nonspecific protein adsorption on peptide-modified GCE surfaces was evaluated using DPV. As shown in Figure 3a and a′, the current response of the PEDOT-citrate/peptide$_3$ surface showed a smaller change compared with that for bare GCE after incubation in negatively charged BSA solution with different concentrations for 30 min. After incubation in positively charged LYS (Figure 3b and b′) and electrically neutral Mb (Figure 3c and c′), there were similar trends in current response changes, indicating good antifouling performance of the designed peptide. Meanwhile, the antifouling property of the three-in-one peptide-modified biosensor was explored in complex human serum. As shown in Figure S7a, the DPV signal changes were recorded before and after incubation in different concentrations of human serum. Clearly, the PEDOT-citrate/peptide surface retained most of their original signal with just a slight decrease (< 5% after incubation in 10% human serum). Long-term antifouling performance of the biosensor in 10% human serum was displayed in Figure S7b, and the results were acceptable. Moreover, to display the antifouling capabilities of parts A and B (Scheme 1), we compared the antifouling performance of peptide$_1$- (without part B), peptide$_2$- (without part A), and peptide$_3$-modified electrodes, respectively. As exhibited in Figure S8, the designed peptide$_3$, including parts A and B, has better antifouling performance than peptide$_1$ and peptide$_2$ after incubation in different concentrations of FBS (fetal bovine serum, a real biological matrix); even after incubation in 50% FBS, the current change of the peptide$_3$-modified film is modulated by < 5.0%. Notably, after incubation in 100% FBS, the antifouling performance of peptide$_3$ was much better than those of the peptide$_1$ and peptide$_2$, ascribed to the synergistic effect of parts A and B.

https://dx.doi.org/10.1021/acs.analchem.9b05299
Anal. Chem. 2020, 92, 5795−5802

The antifouling performances of the modified electrodes were further confirmed by fluorescence microscopy. Clearly, as shown in Figure 4, a lot of fluorescein isothiocyanate-labeled

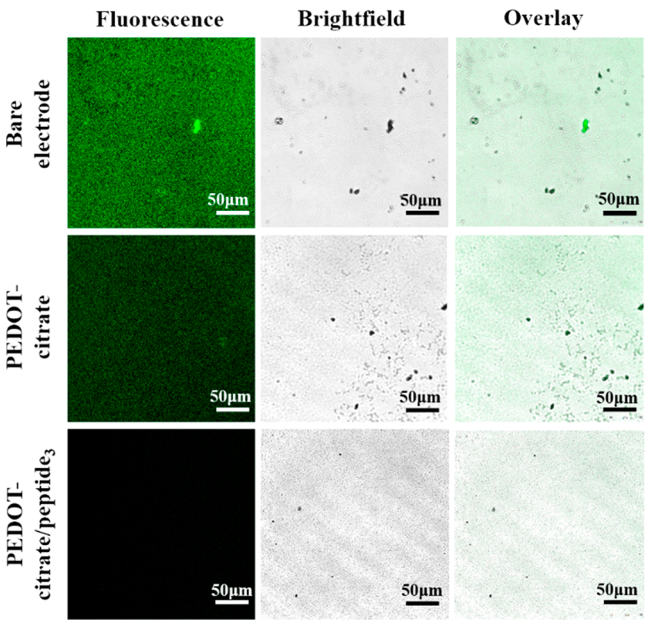

Figure 4. Fluorescence microscopy images of bare GCE, GCE/PEDOT-citrate, and GCE/PEDOT-citrate/peptide$_3$ after incubation in 0.2 mg·mL^{-1} FITC-BSA solution for 2 h.

proteins (FITC-BSA) were adsorbed on the bare (first line) and PEDOT-citrate-coated (second line) electrodes. In contrast, peptide$_3$-coated (third line) electrodes exhibited a relatively clean surface within 2 h. These results clearly indicated that the designed multifunctional peptide displayed excellent protein-repelling ability in single-protein solution and even concentrated complex media of FBS.

Analytical Performances for APN. The detection of APN based on the designed multifunction peptide was performed using DPV, and the peak current signal was directly related to the amount of APN specifically attached on the electrode surface. As displayed in Figure 5a, the current signal decreased gradually with the increase in APN concentration, due to the accumulation of APN on the electrode surface that blocked the electron transfer. A good linear relationship between DPV peak current and the logarithm of the APN concentration within the scope of 1 ng·mL^{-1} to 15 μg·mL^{-1} was obtained (Figure 5b). The limit of detection (LOD, S/N = 3) was calculated to be 0.4 ng·mL^{-1}. Notably, this method exhibited better or comparable linear range and LOD to previous assays (Table S2). The main competitive advantages can be attributed to (1) excellent antifouling property of the three-in-one peptide, especially the two-section collaborative antifouling; (2) specific recognition between peptide and APN; and (3) integration of the anchoring, antifouling, and recognizing capabilities into one peptide, thus avoiding the interference between antifouling materials and sensing probes.

Optical Monitoring of Captured Cells and Cell Detection. To further prove the reliability of cell detection, optical imaging was recorded during the sensing process. Fluorescein diacetate (FDA), which is a live cell-coloring agent, was used to stain the captured HepG2. As exhibited in Figure S9, the fluorescence image of the PEDOT-citrate/

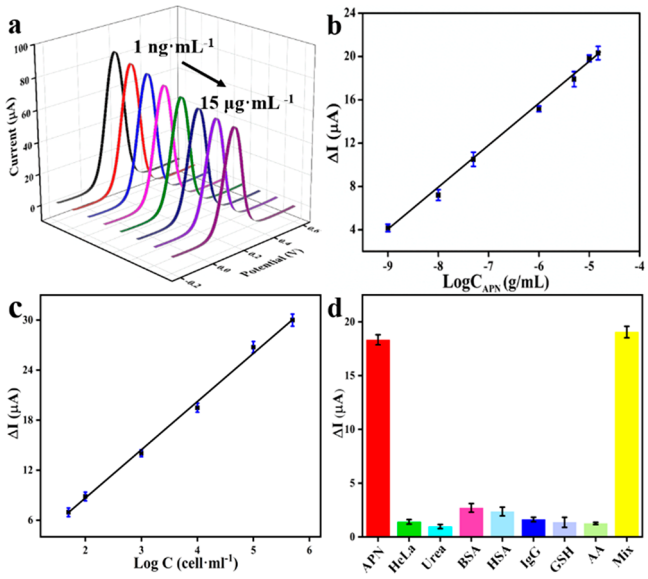

Figure 5. (a) DPV responses of the biosensor interface after being incubated in different concentrations of APN. Calibration curve of the biosensor for APN (b) and HepG2 cell (c) detection. (d) Current change (ΔI) of the APN sensor toward 5 μg·mL^{-1} APN, 1.0 × 10^4 cells·mL^{-1} HeLa cells, 1 mg·mL^{-1} urea, BSA, HSA, IgG, GSH, AA, and their mixture (Mix).

peptide-modified electrode incubated with HeLa cells (as control) was almost black, while that incubated with 1.0 × 10^4 cells·mL^{-1} of HepG2 cells displayed an obvious green fluorescence, indicating that HepG2 cells were captured successfully by the designed peptides. Meanwhile, the fluorescence results also indicated that the designed peptide could resist nonspecific cell adsorption. As can be seen in Figure 5c, within the range of the concentration from 50 to 5 × 10^5 cells·mL^{-1}, the peak current signal decreased linearly with an increase of the logarithm of the cell concentration, with an LOD of 20 cells·mL^{-1} (S/N = 3).

Sensing Performance in Human Urine. The practical application of the biosensor was tested in human urine. Different concentrations of APN were determined by the standard addition method using the developed biosensor, with recoveries from 97.8% to 103.6% and RSD of <3.08% (Table 1), indicating that the biosensor is suitable for APN detection in real samples.

Table 1. APN Detection in Human Urine

sample no.	content[a] (μg/mL)	add (μg/mL)	found[a] (μg/mL)	recovery (%)	RSD (%)
1	0.36	1.00	1.41	103.6	3.08
2	0.32	2.00	2.27	97.8	2.76
3	0.51	5.00	5.43	98.5	2.03

[a]Average of three determinations.

Selectivity, Stability, Reproducibility, and Reusability of the Biosensor. The selectivity of the biosensor was evaluated by recording the current changes in different solutions containing APN, HeLa cells, urea, BSA, HSA, IgG, GSH, AA, and their mixture (Figure 5d). Even in the presence of 1 mg·mL^{-1} interferential reagents and 1.0 × 10^4 HeLa cells, the biosensor showed almost no response, indicating excellent selectivity. The stability of the biosensor was first evaluated by

https://dx.doi.org/10.1021/acs.analchem.9b05299
Anal. Chem. 2020, 92, 5795−5802

continuous CV scan in PBS (10 mM, pH 7.4) containing 5.0 mM $[Fe(CN)_6]^{3-/4-}$ and 0.1 M KCl. As shown in Figure S10a, the current signal remained nearly unchanged after 50 scan cycles. In addition, the biosensor remained >90% of its original current response after being stored at 4 °C in PBS for 15 days (Figure S10d). To evaluate the reproducibility, 1 $\mu g \cdot mL^{-1}$ APN was detected by five independently prepared sensors, and one biosensor was used to detect 1 $\mu g \cdot mL^{-1}$ APN five times. The relative standard deviations (RSDs) were 8.32% and 3.50%, respectively (Figure S10b and c), indicating acceptable reproducibility. The reusability of the biosensor was investigated through a regeneration step. The used APN biosensor was immersed into 6.0 mM NaOH and 0.6% ethanol solution for 10 min and then washed with PBS prior to the next detection. As shown in Figure S11, the current responses showed no significant changes after five repeated regeneration experiments, suggesting an encouraging reusability of the APN biosensor.

CONCLUSIONS

In conclusion, we have designed a new peptide that combined the important functions of anchoring, antifouling, and recognizing, and developed low-fouling electrochemical biosensors for the detection of APN and HepG2. The designed three-in-one peptides were facile for immobilization, and along with the anchoring of the peptides to electrode surfaces, antifouling biosensing interfaces were simply constructed. Electrochemical biosensors based on the designed peptides exhibited excellent stability, selectivity, and high sensitivity (limits of detection were 0.4 $ng \cdot mL^{-1}$ for APN and 20 $cells \cdot mL^{-1}$ for HepG2 cells). More importantly, owing to the unique design of the peptides, the biosensors were capable of detecting targets in the presence of high concentrations of nonspecific proteins as well as in complex biological media. This strategy for the design of a three-in-one peptide to construct antifouling biosensors may be readily extended to a broad range of sensing devices.

ASSOCIATED CONTENT

Supporting Information

The Supporting Information is available free of charge at https://pubs.acs.org/doi/10.1021/acs.analchem.9b05299.

Zeta potential, ATR-FT-IR spectroscopy of peptide, static water contact angles surface electrification evaluation, electrochemical characterization of fabrication process, optimization of sensing conditions, cell incubation and fluorescence microscopy images, and selectivity, stability, and reproducibility of the biosensor (PDF)

AUTHOR INFORMATION

Corresponding Author

Xiliang Luo − *Key Laboratory of Optic-electric Sensing and Analytical Chemistry for Life Science, MOE; Shandong Key Laboratory of Biochemical Analysis; Key Laboratory of Analytical Chemistry for Life Science in Universities of Shandong; and College of Chemistry and Molecular Engineering, Qingdao University of Science and Technology, Qingdao 266042, P. R. China;* orcid.org/0000-0001-6075-7089; Phone: +86 532 84022860; Email: xiliangluo@qust.edu.cn; Fax: +86 532 84022681

Authors

Zhen Song − *Key Laboratory of Optic-electric Sensing and Analytical Chemistry for Life Science, MOE; Shandong Key Laboratory of Biochemical Analysis; Key Laboratory of Analytical Chemistry for Life Science in Universities of Shandong; and College of Chemistry and Molecular Engineering, Qingdao University of Science and Technology, Qingdao 266042, P. R. China*

Min Chen − *Key Laboratory of Optic-electric Sensing and Analytical Chemistry for Life Science, MOE; Shandong Key Laboratory of Biochemical Analysis; Key Laboratory of Analytical Chemistry for Life Science in Universities of Shandong; and College of Chemistry and Molecular Engineering, Qingdao University of Science and Technology, Qingdao 266042, P. R. China*

Caifeng Ding − *Key Laboratory of Optic-electric Sensing and Analytical Chemistry for Life Science, MOE; Shandong Key Laboratory of Biochemical Analysis; Key Laboratory of Analytical Chemistry for Life Science in Universities of Shandong; and College of Chemistry and Molecular Engineering, Qingdao University of Science and Technology, Qingdao 266042, P. R. China*

Complete contact information is available at: https://pubs.acs.org/10.1021/acs.analchem.9b05299

Notes

The authors declare no competing financial interest.

ACKNOWLEDGMENTS

This work is supported by the National Natural Science Foundation of China (21675093 and 21974075) and the Taishan Scholar Program of Shandong Province of China (ts20110829).

REFERENCES

(1) Wang, G. X.; Xu, Q. J.; Liu, L.; Su, X. L.; Lin, J. H.; Xu, G. Y.; Luo, X. L. *ACS Appl. Mater. Interfaces* **2017**, *9* (36), 31153−31160.

(2) Ederth, T.; Lerm, M.; Orihuela, B.; Rittschof, D. *Langmuir* **2019**, *35* (5), 1818−1827.

(3) Cui, M.; Wang, Y.; Jiao, M. X.; Jayachandran, S.; Wu, Y. M.; Fan, X. J.; Luo, X. L. *ACS Sens.* **2017**, *2* (4), 490−494.

(4) Chen, S. F.; Cao, Z. Q.; Jiang, S. Y. *Biomaterials* **2009**, *30* (29), 5892−6.

(5) Sakala, G. P.; Reches, M. *Adv. Mater. Interfaces* **2018**, *5* (18), 1800073.

(6) Cui, M.; Song, Z. L.; Wu, Y. M.; Guo, B.; Fan, X. J.; Luo, X. L. *Biosens. Bioelectron.* **2016**, *79*, 736−741.

(7) Sun, K.; Song, L. S.; Xie, Y. N.; Liu, D. B.; Wang, D.; Wang, Z.; Ma, W. S.; Zhu, J. S.; Jiang, X. Y. *Langmuir* **2011**, *27* (10), 5709−5712.

(8) Liu, N. Z.; Song, J. Y.; Lu, Y. W.; Davis, J. J.; Gao, F. X.; Luo, X. L. *Anal. Chem.* **2019**, *91* (13), 8334−8340.

(9) Sharma, S.; Johnson, R. W.; Desai, T. A. *Biosens. Bioelectron.* **2004**, *20* (2), 227−239.

(10) Knowles, B. R.; Wagner, P.; Maclaughlin, S.; Higgins, M. J.; Molino, P. J. *ACS Appl. Mater. Interfaces* **2017**, *9* (22), 18584−18594.

(11) Song, Z.; Sheng, G.; Cui, Y. G.; Li, M. R.; Song, Z. L.; Ding, C. F.; Luo, X. L. *Microchim. Acta* **2019**, *186* (4), 220.

(12) Ran, J.; Wu, L.; Zhang, Z. H.; Xu, T. W. *Prog. Polym. Sci.* **2014**, *39* (1), 124−144.

(13) Asuri, P.; Karajanagi, S. S.; Kane, R. S.; Dordick, J. S. *Small* **2007**, *3* (1), 50−53.

(14) Nowinski, A. K.; Sun, F.; White, A. D.; Keefe, A. J.; Jiang, S. Y. *J. Am. Chem. Soc.* **2012**, *134* (13), 6000−6005.

(15) Liu, N. Z.; Hui, N.; Davis, J. J.; Luo, X. L. *ACS Sens.* **2018**, *3* (6), 1210−1216.
(16) Liu, N. Z.; Xu, Z. Y.; Morrin, A.; Luo, X. L. *Anal. Methods* **2019**, *11* (6), 702−711.
(17) Wang, G. X.; Su, X. T.; Xu, Q. J.; Xu, G. Y.; Lin, J. H.; Luo, X. L. *Biosens. Bioelectron.* **2018**, *101*, 129−134.
(18) Li, N.; Yue, X. F.; Zhang, L.; Wang, K.; Zhang, J.; Zhang, Z. Q.; Dang, F. Q. *J. Mater. Chem. B* **2019**, *7* (14), 2242−2246.
(19) Gerber, E. E.; Gallo, E. M.; Fontana, S. C.; Davis, E. C.; Wigley, F. M.; Huso, D. L.; Dietz, H. C. *Nature* **2013**, *503* (7474), 126−130.
(20) Englund, E. A.; Wang, D. Y.; Fujigaki, H.; Sakai, H.; Micklitsch, C. M.; Ghirlando, R.; Martin-Manso, G.; Pendrak, M. L.; Roberts, D. D.; Durell, S. R.; Appella, D. H. *Nat. Commun.* **2012**, *3*, 614.
(21) Zhang, Y. X.; Carbonell, R. G.; Rojas, O. J. *Biomacromolecules* **2013**, *14* (12), 4161−4168.
(22) Kish, W. S.; Naik, A. D.; Menegatti, S.; Carbonell, R. G. *Ind. Eng. Chem. Res.* **2013**, *52* (26), 8800−8811.
(23) Wang, W. Z.; Wei, Z. W.; Zhang, D.; Ma, H. L.; Wang, Z. H.; Bu, X. L.; Li, M. L.; Geng, L. L.; Lausted, C.; Hood, L.; Fang, Q. J.; Wang, H.; Hu, Z. Y. *Anal. Chem.* **2014**, *86* (23), 11854−111859.
(24) Wong, A. H. M.; Zhou, D. X.; Rini, J. M. *J. Biol. Chem.* **2012**, *287* (44), 36804−36813.
(25) Shim, J. S.; Kim, J. H.; Cho, H. Y.; Yum, Y. N.; Kim, S. H.; Park, H.-J.; Shim, B. S.; Choi, S. H.; Kwon, H. J. *Chem. Biol.* **2003**, *10* (8), 695−704.
(26) Fontijn, D.; Duyndam, M. C. A.; van Berkel, M. P. A.; Yuana, Y.; Shapiro, L. H.; Pinedo, H. M.; Broxterman, H. J.; Boven, E. *Br. J. Cancer* **2006**, *94* (11), 1627−1636.
(27) Tokuhara, T.; Hattori, N.; Ishida, H.; Hirai, T.; Higashiyama, M.; Kodama, K.; Miyake, M. *Clin. Cancer Res.* **2006**, *12* (13), 3971−3978.
(28) Mawrin, C.; Wolke, C.; Haase, D.; Krüger, S.; Firsching, R.; Keilhoff, G.; Paulus, W.; Gutmann, D. H.; Lal, A.; Lendeckel, U. *Brain Pathol.* **2010**, *20* (1), 200−210.
(29) Cui, S. X.; Qu, X. J.; Gao, Z. H.; Zhang, Y. S.; Zhang, X. F.; Zhao, C. R.; Xu, W. F.; Li, Q. B.; Han, J. X. *Cancer Lett.* **2010**, *292* (2), 153−162.
(30) Hata, R.; Nonaka, H.; Takakusagi, Y.; Ichikawa, K.; Sando, S. *Angew. Chem., Int. Ed.* **2016**, *55* (5), 1765−1768.
(31) Terauchi, M.; Kajiyama, H.; Shibata, K.; Ino, K.; Nawa, A.; Mizutani, S.; Kikkawa, F. *BMC Cancer* **2007**, *7* (1), 140.
(32) He, X. Y.; Xu, Y. H.; Shi, W.; Ma, H. M. *Anal. Chem.* **2017**, *89* (5), 3217−3221.
(33) Li, H. D.; Li, Y. Q.; Yao, Q. C.; Fan, J. L.; Sun, W.; Long, S.; Shao, K.; Du, J. J.; Wang, J. Y.; Peng, X. J. *Chem. Sci.* **2019**, *10* (6), 1619−1625.
(34) Wang, J. J.; Xu, G. Y.; Wang, W.; Xu, S. H.; Luo, X. L. *Chem. - Asian J.* **2015**, *10* (9), 1892−1897.
(35) Wang, G. X.; Han, R.; Su, X. L.; Li, Y. N.; Xu, G. Y.; Luo, X. L. *Biosens. Bioelectron.* **2017**, *92*, 396−401.

https://dx.doi.org/10.1021/acs.analchem.9b05299
Anal. Chem. 2020, 92, 5795−5802